MIT Libraries | DSpace@MIT

MIT Open Access Articles

PVTX characteristics of oil inclusions from Asmari formation in Kuh-e-Mond heavy oil field in Iran

The MIT Faculty has made this article openly available. ***Please share*** how this access benefits you. Your story matters.

Citation: Shariatinia, Zeinab et al. "PVTX Characteristics of Oil Inclusions from Asmari Formation in Kuh-E-Mond Heavy Oil Field in Iran." International Journal of Earth Sciences 104.3 (2015): 603–623.

As Published: http://dx.doi.org/10.1007/s00531-014-1101-y

Publisher: Springer Berlin Heidelberg

Persistent URL: http://hdl.handle.net/1721.1/104941

Version: Author's final manuscript: final author's manuscript post peer review, without publisher's formatting or copy editing

Terms of Use: Article is made available in accordance with the publisher's policy and may be subject to US copyright law. Please refer to the publisher's site for terms of use.

Massachusetts Institute of Technology

Int J Earth Sci (Geol Rundsch) (2015) 104:603–623
DOI 10.1007/s00531-014-1101-y

ORIGINAL PAPER

PVTX characteristics of oil inclusions from Asmari formation in Kuh-e-Mond heavy oil field in Iran

Zeinab Shariatinia · Manouchehr Haghighi · Ali Shafiei · Sadat Feiznia · Sohrab Zendehboudi

Received: 5 March 2012 / Accepted: 31 October 2014 / Published online: 10 December 2014
© Springer-Verlag Berlin Heidelberg 2014

Abstract Incorporating PVT properties and compositional evolution of oil inclusions into reservoir engineering simulator protocols can enhance understanding of oil accumulation, reservoir charge history, and migration events. Microthermometry and volumetric analysis have proven to be useful tools in compositional reconstitution and PT studies of oil inclusions and were used to determine composition, thermodynamic conditions, physical properties, and gas-to-oil ratios of heavy oil samples from Asmari carbonate reservoir in Kuh-e-Mond heavy oil field in Iran. PVT properties were predicted using a PVT black-oil model, and an acceptable agreement was observed between the experiments and the simulations. Homogenization temperatures were determined using microthermometry techniques in dolomite and calcite cements of the Asmari Formation, as well. Based on the homogenization temperature data, the undersaturated hydrocarbon mixture prior to formation of the gas cap migrated with a higher gas-to-oil ratio from a source rock. According to the oil inclusion data, the onset of carbonate cementation occurred at temperatures above 45 °C and that cementation was progressive through burial diagenesis. PVT black-oil simulator results showed that the reservoir pressure and temperature were set at 100 bar and 54 °C during the initial stages of oil migration. Compositional modeling implies that primary and secondary cracking in source rocks were responsible for retention of heavy components and migration of miscible three-phase flow during hydrocarbon evolution. The PT evolution of the petroleum inclusions indicates changes in thermodynamic properties and mobility due to phenomena such as cracking, mixing, or/and transport at various stages of oil migration.

Keywords Petroleum inclusions · Compositional history · PVT properties · Black-oil simulator · Kuh-e-Mond heavy oil field

List of symbols

% dev	Total mole fraction of components with C_n carbon atoms
A	Constant defined in Eq. 2
ABS	Average absolute deviation
c_1–c_4	Coefficients defined in Eq. 3
CLSM	Confocal laser scanning microscopy
C_n	Carbon number
cP	Centi Poise
d_1–d_4	Coefficients defined in Eq. 4
e_1–e_4	Coefficients defined in Eq. 5
F_V	Bubble filling degree (%) (volume of vapor in %)
GOR	Gas-to-oil ratio (SCF/STBO for oil reservoir and kg-gas/kg-oil for the oil inclusions)
m	Function of the acentric factor
MW	Molecular weight
Mw,7+	Molar weight of the C_{7+} fraction (g/mol)

Z. Shariatinia (✉) · M. Haghighi
Department of Geosciences, University of Tehran, Tehran, Iran
e-mail: zshariatinia@yahoo.com

M. Haghighi
Australian Schools of Petroleum, University of Adelaide, Adelaide, SA, Australia

A. Shafiei (✉)
Department of Earth and Environmental Sciences, University of Waterloo, Waterloo, ON, Canada
e-mail: geomekker@gmail.com

S. Feiznia
College of Natural Resources, University of Tehran, Tehran, Iran

S. Zendehboudi
Department of Chemical Engineering, Massachusetts Institute of Technology, Cambridge, MA, USA

n	Number of observations
P	Pressure (bar)
P_c	Critical pressure (bar)
P_H	Homogenization pressure (bar)
T	Temperature (°C)
T_H	Homogenization temperature (°C)
X_i	X-value of ith observation
Y_i	Y-value of ith observation
Z_n	Total mole of components
ρ	Density in g/cm^3 at 15 °C and 1 atm
ω	Acentric factor

Introduction

Integration of PVT properties and compositional evolution of petroleum inclusions into reservoir engineering simulator protocols further understanding of petroleum generation and emplacement, reservoir charge history, and the nature of migration events (Munz 2001; Thiéry et al. 2002; Tseng et al. 2002). Petroleum geologists use core samples and hydrocarbon mixtures at surface conditions to explore hydrocarbon migration in sedimentary basins (Bigge et al. 1995; Aplin et al. 1999, 2000). One approach to determine the initial composition and also reconstruct the basin migration history is studying fluids trapped in inclusions within diagenetically formed minerals such as quartz, calcite, dolomite, and fluorite (Thiéry et al. 2000). Oil is trapped in inclusions during filling of a reservoir or along a migration path; thus, petroleum inclusions are considered as doors to the past, representing paleocompositions and PT conditions at the time of entrapment (Bigge et al. 1995; Bodnar 1999; Aplin et al. 1999, 2000; Adams et al. 2006). Petroleum inclusions are first investigated by petrographic methods to delineate their connections to the host mineral. The petrographic description is normally followed by a systematic microthermometric analysis to determine phase transitions (Munz 2001). Various hypotheses related to inclusion chronology and homogenization temperatures of hydrocarbon mixtures were proposed in the literature (England 1990; Bodnar 1999; Burruss 1991, 1992; Dubessy et al. 2001). The study of fluid inclusions is of great value in reconstructing petroleum composition and PT evolution of migrating hydrocarbons. However, the interpretation of simulation data is not easy nor straightforward (Glasø 1980; Burruss 1991, 1992; England 1990; Jones et al. 1996; George et al. 1996, 2007; Bodnar 1999).

Microthermometry involves determining homogenization temperature (T_H) followed by volumetric determination of vapor fraction (F_V) at different temperatures. Then, homogenization pressure (P_H) can be estimated using thermodynamic modeling. This is an aid to determine the entrapped hydrocarbon composition, which cannot be specified uniquely by microthermometry and volumetric techniques alone. For this reason, an appropriate compositional model for natural petroleum mixtures should be used so that composition indeterminacy can be reduced using an iterative procedure where the assumed oil composition is adjusted to match the modeled T_H and F_V with the measured values. The last stage in microthermometry is to compute the trapping parameters such as trapping pressure (P_T) and trapping temperature (T_T) (England 1990,1991 ; George et al. 1996, 2007; Dubessy et al. 2001).

An inclusion is considered as a closed system. Hence, its bulk density is assumed constant. Bulk density of a particular petroleum inclusion is a function of the individual densities of the liquids and vapor phases of the mixture (Standing 1952; Starling and Powers 1970; Roedder 1984a, b; Pedersen et al. 1984, 1989; Stasiuk and Snowdon 1997; Swarbrick et al. 2000). Pironon et al. (1998 and Aplin et al. 1999) reported investigation of physical properties of hydrocarbon components in oil inclusions through volumetric reconstruction of fluorescent fluid inclusions. They used confocal laser scanning microscopy (CLSM) method to approximate the magnitude of the vapor volume fraction at room conditions (Osjord et al. 1985; Macleaod et al. 1994; Bigge et al. 1995; Lisk et al. 1996; Aplin et al. 1999, 2000).

Several geological and geochemical studies are reported on petroleum inclusions to account for variations arising from multiple petroleum sources, several phases of fluid charging, and internal changes in hydrocarbon pool composition. Due to the fact that inclusions are not affected by such variations, they can provide a clear picture of the reservoir fluids at the time of entrapment helping to deconvolve the reservoir charge history (Glasø 1980; Roedder 1984a, b; Karlsen et al. 1993; Jones et al. 1996, 2000; Kamali and Rezaee 2003; George et al. 2001, 2007). It is widely accepted that natural petroleum inclusions record physical conditions predating the reservoir alterations that may have taken place after the inclusion was sealed. Several researchers have employed re-equilibrated inclusions data to describe post-entrapment occurrences. For instance, it was shown that homogenization temperature (T_H) of re-equilibrated fluid inclusions can be used to determine the highest temperature at the time that the maximum burial happens (Standing 1952; Starling and Powers 1970; Lin et al. 1972; Roedder 1984a, b; Pedersen et al. 1984, 1989; Osjord et al. 1985; Macleaod et al. 1994; Lisk et al. 1996; Stasiuk and Snowdon 1997).

Scientists generally look at petroleum accumulations in terms of simple models such as dry gas, wet gas, condensate gas, critical fluid state, light oil, and heavy oil. This general classification of hydrocarbon reservoir types is based on the chemical and physical characterization of the petroleum mixtures with emphasis on evolution to other

compositions such as reduction in light alkane content and increase in heavy components associated with diffusion and biodegradation (Katz et al. 1943; Lin et al. 1972; Karlsen et al. 1993; Larter et al. 2006). Studies such as the analysis of Ula field in North Sea (Aplin et al. 1999) (Brent formation) and the detailed analysis of oil sands in Canada (Hassanzadeh et al. 2008; Larter et al. 2008) have had enhanced accuracy and computational efficiency of black-oil reservoir simulations. The black-oil PVT method appears to be reasonably reliable for prediction of thermodynamic properties of the petroleum trapped in fluid inclusions (Standing 1952; Starling and Powers 1970; Roedder 1984a, b; Pederson et al. 1984, 1989; Stasiuk and Snowdon 1997; Swarbrick et al. 2000; Thiéry et al. 2000; Tseng et al. 2002; Volk et al. 2002). The black-oil PVT simulation software uses proper thermodynamic correlations and equation of state (EOS) to compute pressure, mole fractions, and phase behavior for a hydrocarbon mixture consisting of two liquid phases and one gas phase. The black-oil PVT module can simulate the phase envelopes and isochores based on the composition values available from the field operators. PVT properties can then be integrated with compositional evolution of petroleum inclusions using well-accepted reservoir engineering simulator protocols.

Oil inclusions resolve into multiple subsets as evidenced by primary oil inclusions from first-stage calcite cements and the last-stage calcite and dolomite fracture-healed cements. "Tar spots" and "solid bitumen segregations" were found on the walls of petroleum inclusions in water and petroleum interface. "Tar spots" precipitation could be as a result of isochemical changes after trapping (Roedder 1984a, b). In addition, polar heterocyclic compounds tend to be trapped more easily than pure hydrocarbons. The stronger adsorption of these compounds on mineral surface leads to an enrichment of polar compounds relative to their parent oils (e.g., Macleod et al. 1993, 1994; Nedkvitne et al. 1993; Pang et al. 1998).

In this paper, microthermometry and PVTX simulations were used to delineate thermodynamic conditions, physical properties, and composition of heavy oil samples from Asmari formation reservoir which forms part of the Kuh-e-Mond heavy oil field in SW Iran. Homogenization temperature (T_H) was determined using microthermometry on inclusions found in dolomite and calcite cements of this carbonate formation. Volumetric PVT tests were carried out to determine mixture composition, gas-to-oil ratio (GOR), and other thermodynamic properties of the heavy crude oil. A PVT black-oil module was also used, taking into account the initial composition over time after migration, to estimate compositional history and PVT properties of the inclusions. Molar volume, GOR, and T_H were the input parameters for the simulator to predict thermodynamic state of the petroleum mixtures. The simulator uses an iterative procedure to obtain the best match to the properties of the hydrocarbon samples from representative well(s).

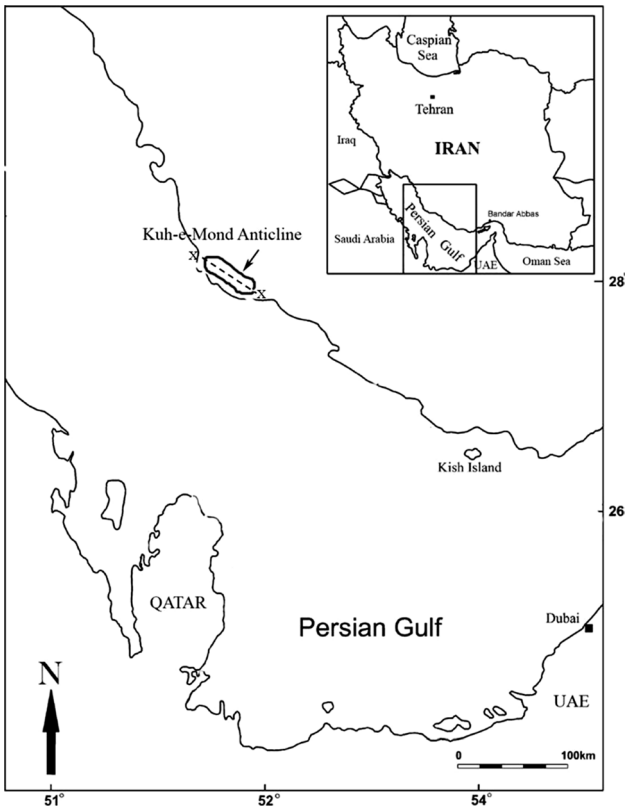

Fig. 1 Geographical location of the Kuh-e-Mond heavy oil field located in SW Iran. Cross section XX along the axis of the Kuh-e-Mond anticline is presented in Fig. 2

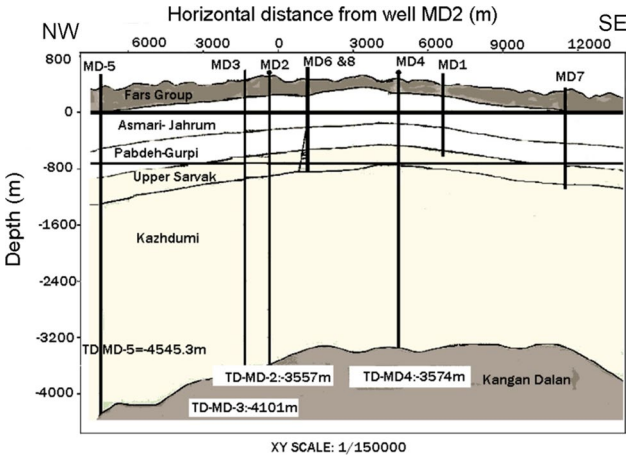

Fig. 2 Geological cross section along the XX line (Fig. 1), which is also the axis of the Kuh-e-Mond anticline and location of the wells in the field. Fluid inclusion samples for this study were taken from MD6 well and are from Asmari and Jahrum formations. The depth of sampling varies from 300 to 735 m as shown in Fig. 4

Kuh-e-Mond heavy oil field

Kuh-e-Mond (Fig. 1) is the largest on shore heavy oil field in Iran, found in a giant anticline with a NW–SE trend, parallel to the Zagros orogenic belt. The field was first discovered in 1931, and a systematic exploration began in 1984. This relatively symmetrical anticline is 90 km long and 16 km wide with an estimated minimum heavy oil resource base of 6 billion barrels of oil originally in place (OOIP) and oil viscosities of 570–1,160 cP in situ. A large number of faults cut the axial plane of the structure causing some strata displacements around the central and plunging parts of the structure. The average dip of the southwest and northeast flanks of the anticline is 17° and 15°, respectively (Moshtaghian et al. 1988; Shafiei et al. 2007). Heavy oil occurrence has been confirmed in three separate fractured carbonate formations, the Asmari, Jahrum (Eocene), and Sarvak (Cretaceous) formations (Figs. 2, 3). The trap structure was formed during the main phase of the Zagros folding in late Miocene and Pliocene, as shown by the relatively constant thickness of the lower Miocene succession (Moshtaghian et al. 1988; Kamali and Rezaee 2003).

According to petrophysical evaluations, the Asmari formation limestone is a poor reservoir; only part of it has good porosity (ϕ) in the range of 24–31 % with water saturation (S_w) around 20 %. The Jahrum formation, a reservoir of Eocene age, mainly consists of highly fractured, light-brown medium-grained crystalline dolomite with intercrystalline vuggy and fracture porosity. The lower Jahrum is mainly white detrital dolomitic and partly anhydritic and cherty limestone. This formation contains immobile heavy oil. Original volume of oil in place has been estimated at ~3 billion barrels (Bashari 1988; Moshtaghian et al. 1988). The Cenomanian Sarvak formation is mainly composed of highly fractured marly neritic and pelagic limestone with interbedded shale layers. This formation is divided into three main units: upper, middle, and lower Sarvak. The upper unit consists of clean limestone with some slightly argillaceous zones. In the middle Sarvak, shale and marls are dominant. Lower Sarvak is mainly composed of marly limestone with some shale bed intercalations. During drilling, heavy mud losses were reported in Sarvak formation indicating a highly fractured formation. The Sarvak heavy oil reservoir contains an estimated (Original Oil In Place) OOIP of 3.6 billion barrels (Moshtaghian et al. 1988).

The source rock has not been identified yet. Determining the source rock requires comprehensive source oil correlations. The cap rock is the Gachsaran evaporate formation of Middle to Late Miocene-Oligocene (Motiei 1994). It has also been speculated that the Gachsaran Formation was syntectonic sediment deposited in NW-trending synclinal troughs (during active folding) that divided the Zagros foreland basin into sub-basins with poor water circulation (Hessami et al. 2001). However, this picture contrasts with suggestions that the Gachsaran Formation was deposited in very shallow lagoon and sabkha environment of arid climates (Gill and Ala 1972; Motiei 19931993; Bahroudi and Koyi 2004). The organic content of reservoir oil including TOC, HI, and type of organic matter is well described in Kamali and Rezaee (2003).

Fluid inclusions studies

Fluid inclusions (FI) are defined as micron-scale, fluid-filled occluded cavities formed during cementation or fracture healing events (McQuillan 1985; Ahmadhadi et al. 2007). Inclusions generally remain intact once formed and are thus a record of temperature, pressure, and composition associated with hydrocarbon migration and charging at the time of formation. Hydrocarbons trapped in fluid inclusions can be extracted and analyzed via mass spectrometry. Petrographic studies of oil inclusion distributions also help delimit timing and migration pathways for fluid charging and later fluid migration events (Munz 2001). Coupled with compositional data, these techniques enable assessing oil charge histories based on the measurable data, which in turn can help construct and evaluate more theoretical and general models of the regional hydrocarbon generation and flow.

Sample preparation and methodology

The samples used for the purpose of this study were taken from the Asmari and Jahrum formations (MD6 well), which are typical of carbonate platform environment deposits in which calcite, dolomite, and anhydrite are deposited, periodically. Depth of sampling, formation name, texture, and lithology of the samples is presented in Fig. 4. Diagenetic cements including calcite and dolomite affected the whole section and filled the fractures, fossil molds, and cavities. All of them contain oil inclusions. Total of 20 samples from various depths with different sedimentological textures were selected and analyzed for fluid inclusions microthermometry. The analyzed samples then were classified in eight groups of oil inclusions with distinctive characteristics recognized (Table 1). The approach recommended by George et al. (2007) was followed during sample preparation for the purpose of fluid inclusion studies.

Microthermometry

Fluid inclusion microthermometric results are presented in Figs. 5, 6 and Table 1. The rock wafers used were obtained for every single paragenetic generation found in dolomite

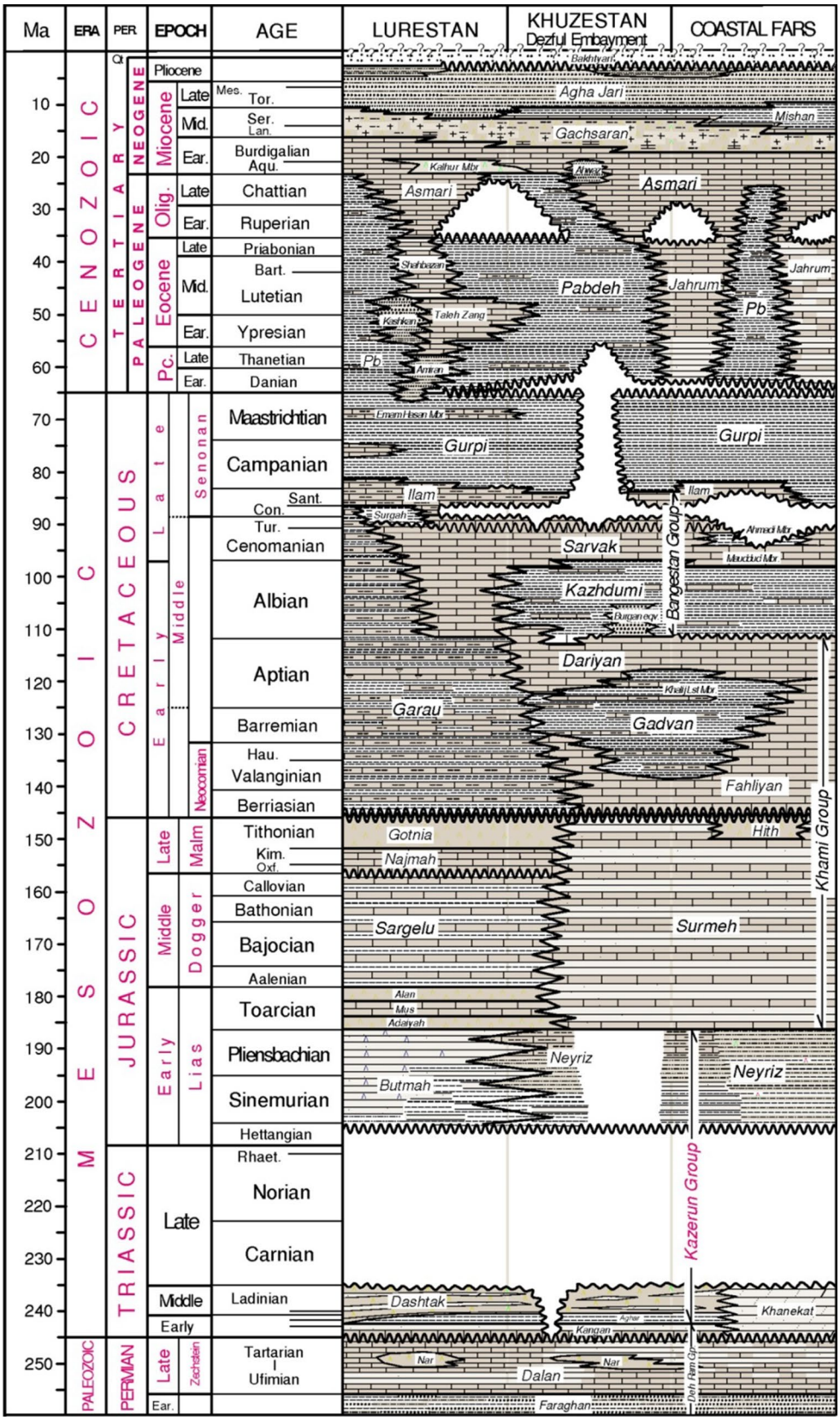

Fig. 3 Lithostratigraphic column of the reservoirs at the Kuh-e-Mond heavy oil field (From Kamali and Rrezaee 2003 after James and Wynd 1965)

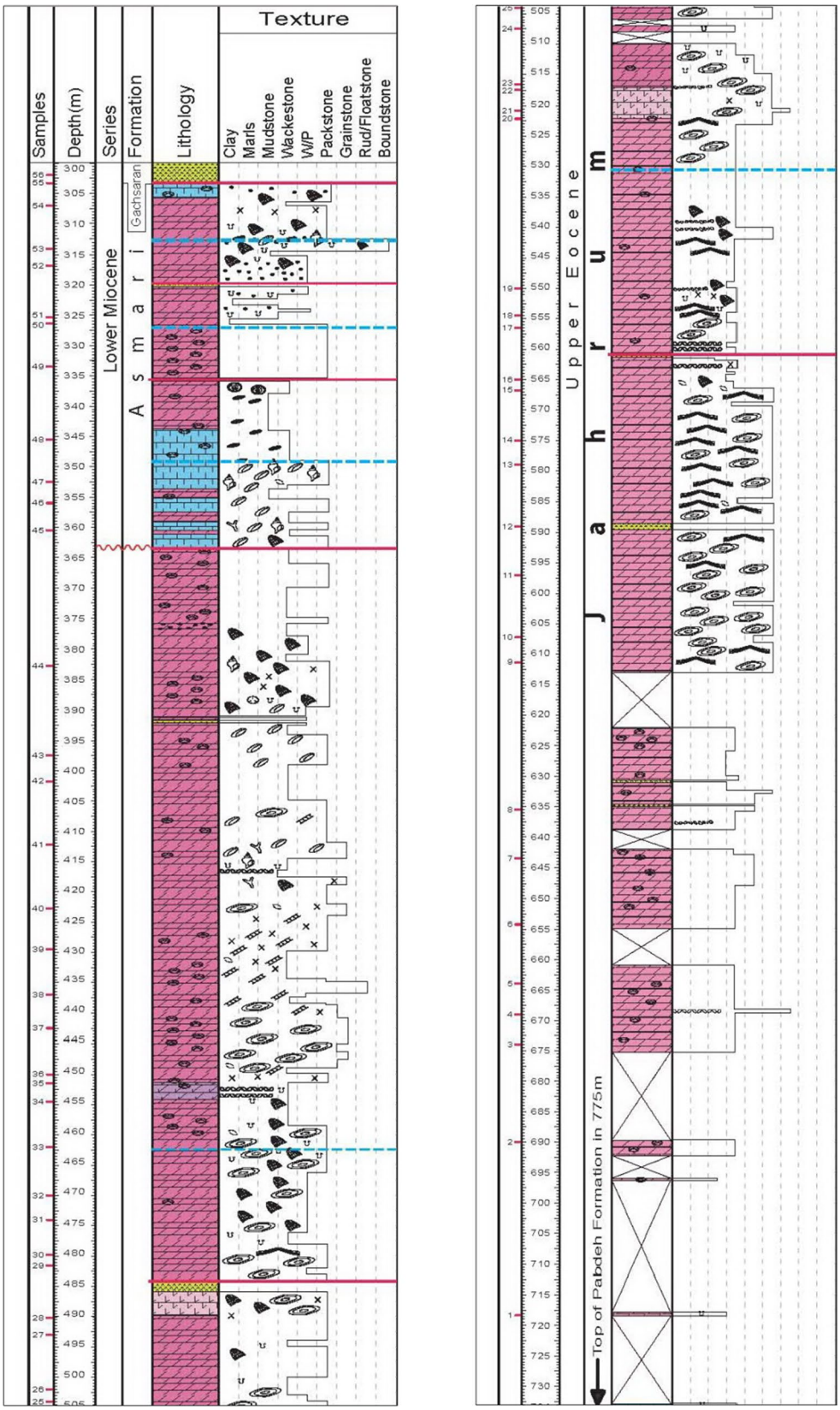

Fig. 4 Depth of sampling, formation name, texture, and lithology of the samples taken from MD6 well (see Fig. 2 for the well location) at the Kuh-e-Mond heavy oil field

Table 1 Summary of "Homogenization temperatures" (T_H) for the samples studied from the Asmari formation

Formation	Sample name	Depth (m)	Host	Inclusion content and type	T_H ranges (°C)	$\mu = \mathfrak{E}x_i{*}n/N$ °C (Gaussian maximum distribution)	Frequency of inclusions (n)	Salinity (wt% eq. NaCl)
Asmari Fm.	ZSH55		Anhydrite	Primary oil	16–24	20	10	
				Secondary oil	24–32	27	11	
	ZSH54		Equant calcite	Primary aqueous	38.8–53.3	43	5	19.1–20
				Primary oil	28–58	52	11	
	ZSH52	316.80	Calcite fossil cavity	Primary oil	40–73	64	17	
				Secondary oil	40–70	51	21	
				Secondary oil (yellow fluorescence)	44.7–64.9	53.6	20	
				Secondary oil (blue UV color)	39.2–78	48	23	
				Primary aqueous	52.3–68.7–76.9–88–98–125.2	103.2	94	19
	ZSH48	335	Calcite fossil cavity	Secondary	45–73	47	20	6.4–18
				Aqueous				
Jahrum Fm.	ZSH29	481.5	Dolomite rim cement	Primary oil	32–67.7	57.5	20	
				Primary aqueous	71–116; 86–117	90.5	14	18.8–20.5
				Secondary aqueous	41–64	58	11	19.1
	ZSH27	493	Sparry calcite vein	Primary oil	32.3–67.7	57.2	40	
				Secondary oil	20–28–53	32	10	
				Primary aqueous	38–44–45–53–75–83	62.9	25	18.1–20.0
				Primary aqueous (coarser calcite crystals)	69–91	77	25	17.2–17.8
	ZSH23	517	Dolomite vein/fracture fill	Primary oil	67.7–124.1	106	29	
				Secondary oil	65–104	85	20	
				Primary aqueous	87.6–104.6	94	100	17.7–19.3
				Secondary aqueous	102–125	119	36	19.8–21.3
	ZSH20	522.10	Anhydrite lath	Primary aqueous	47–59–70	53	30	17.3
				Primary oil	16–20–46	32	29	
			Calcite vein fill	Primary oil <75 °C	50–58	54	10	
				Primary oil >75 °C	110–130	125	9	
				Secondary oil	48–112	66	60	
				Primary aqueous	52–76–83	69.5	12	18–20
				Primary aqueous	50–68.8	61	24	17.7–18.4
	ZSH14	575		Primary aqueous	106–109	107	3	18.9
				Secondary aqueous	70–90	77	14	17.2–17.8
	ZSH12	589	Calcite cavity fill	Primary aqueous	86–107	65	23	20
				Secondary oil	50–65	54	30	
	ZSH4	669	Anhydrite vein fill	Primary oil	41–50	43	6	
				Secondary oil	39–45	39	5	
				Primary aqueous	45–55	50	3	17
			Calcite isopachous equant	Primary aqueous	38.8–53.3		5	
				Primary oil	28–58		11	

(coarse sparry calcites and vein filling), calcite (sparry, vein filling, and fossil cavity), and anhydrite. Moreover, special care was taken in selecting defect-free crystals with no visible evidence of post-entrapment deformation. Fluid inclusion assemblages were interpreted in terms of origin to be primary (isolated or along growth zones) and secondary (trapped along fracture and cleavage planes). The origin and characteristic of the fluids (brines) migrated to the reservoir and precipitated in the fractures as fracture-filling cements can be investigated through analysis of aqueous inclusions found in the cements. In case, sharp differences exist, then it can be concluded that different fluid regimes were active and dominant during the course of hydrocarbon accumulation in the reservoir. The focus of this work was on oil trapped as one phase in a certain time and condition.

PVT simulation of the oil inclusions

Oil inclusions are complex mixtures, which usually contain thousands of different molecules of paraffins, naphthenes, and aromatics. Constituent distributions are not easy to fully describe by standard chemical analysis methods (Horsfield and McLimans 1984; Pedersen et al. 1992; Karlsen et al. 1993; George et al. 2007). Modeling hydrocarbons behavior is feasible if "raw compositions" were known. Hence, using a simulation approach which only requires a small number of representative compositional and physicochemical parameters is inevitable. Such PVT simulators should also be able to satisfactorily model the physicochemical behavior of the mixture of natural hydrocarbons found in the fluid inclusions (Aplin et al. 1999; Ping and Thiéry 2002; Jauber and Mutelet 2004). The main issue here is reconstruction of the phase diagram and the isochore of the entrapped oil from T_H and F_V values. The oil industry encounters similar issues prior to production from an oil reservoir (Ping and Thiéry 2002; Thiéry et al. 2002; Jauber and Mutelet, 2004). For a safe and effective production scheme, thermodynamic parameters and PT envelope of the fluid mixture in the formation should be determined (Munz et al. 1999a, b).

Presence of water in petroleum inclusions should be considered in calculation of isochores (England et al. 1987; Bakker and Jansen 1990, 1991, 1994; Hall and Sterner 1993). Hydrocarbon inclusions can hold a great amount of water, and the invisible aqueous film wetting the walls can be up to 25 % of the molar fraction of the bulk composition of an inclusion. The difference between the thermal expansivity of the aqueous phase and the petroleum becomes considerable above 100 °C and can affect the trapping pressure assessment. For instance, Bodnar (1999) reported that water in fluid inclusions, although invisible, can significantly influence trapping pressures estimates. To avoid large errors in isochore calculation in this study, data from primary oil inclusions (containing hydrocarbons only) were selected to estimate the internal pressure of the inclusions. Then, an estimated trapping pressure was used to determine the physical properties such as pressure and composition of the isopleths and isochores for the hydrocarbon inclusions at the time of trapping. The inclusions were composed of various amounts of gas and oil produced through the heterogeneous trapping process. At these PT conditions, the petroleum does not develop into a homogeneous mixture of gas (5 vol%) and oil (95 vol%).

PVT properties and trapping pressure

To obtain PVT properties of oil inclusions using a PVT simulator, the following important parameters are required:

1. Homogenization temperature of the hydrocarbon mixture,
2. Gas-to-oil ratio (GOR), and
3. Mixture composition that dictates the type of petroleum mixture, the shape of the PT diagram, and the critical properties of the mixture.

Figure 7 shows a typical PT diagram for a multi-component mixture. The critical point (CP) is located at the intersection of two curves, namely the bubble-point curve and the dew-point curve. The isopleth defines the liquid domain (above the bubble-point curve), the gas domain (below the dew-point curve), and the two-phase domain (inside the isopleth). In two-phase domain, the curves (20, 40 %, etc.) are associated with constant magnitudes of the vapor volume fraction (Di Primio et al. 1998).

The PT path of the inclusion is described by an isochore. The three points of interest are the (P_T, T_T) trapping point, the (P_H, T_H) homogenization point, and the (P_V, T_V) point at which the bubble filling degree (F_V) is measured (Aplin et al. 1999; Ping and Thiéry 2002; Thiéry et al. 2002; Thiéry 2006). The PT diagram of a fluid inclusion follows iso-bulk density lines or isochores, first in the two-phase domain and then in the single-phase domain (Fig. 7). The transition temperature between the two-phase and single-phase zones is called homogenization temperature (T_H). Homogenization can happen into the liquid or the gas state but less commonly at the critical condition (Goldstein and Reynolds 1994).

Homogenization temperature

Homogenization temperature (T_H) of a particular petroleum inclusion refers to the minimum temperature of entrapment of the fluid in a formation (Parnell et al. 2001; Parnell 2010). This specific temperature determination along with other geochemical methods limits possible sources and migration pathways (or/and direction) for diagenetic hydrocarbons. Hence, it provides a constraint on geologic setting for

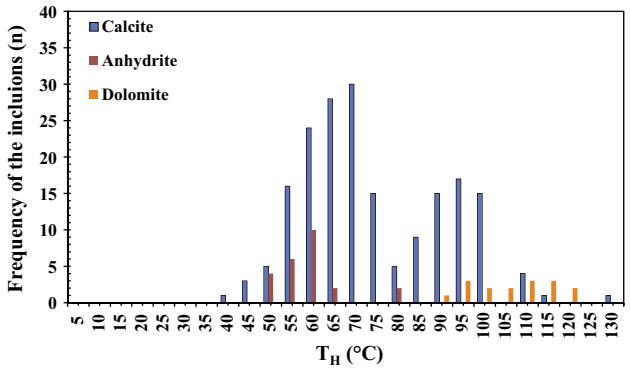

Fig. 5 T_H versus frequency of the inclusions trapped in dolomite, calcite, and anhydrite cements from the Asmari formation. Homogenization temperatures are grouped by mineralogy here

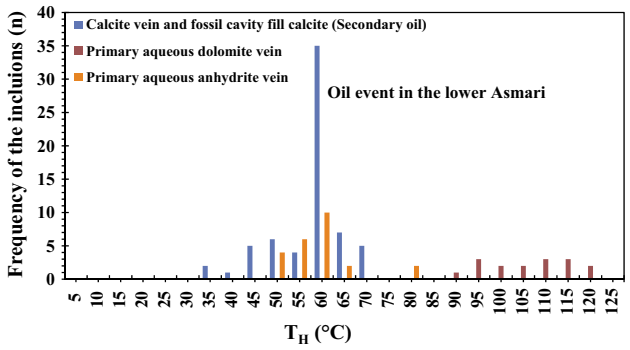

Fig. 6 Distribution of T_H of aqueous inclusions trapped in dolomite and calcite fracture-filling cements from upper and middle Asmari formation

diagenesis. T_H can be affected by trapping and post-trapping conditions and processes, as well as sample preparation. These factors are the main concerns with respect to the reliability of data for petroleum inclusions analysis. The minimum temperature of trapping is normally determined using the microthermometry technique (Bodnar and Bethke 1984; Goldstein 1986). The T_H values for the Kuh-e-Mond petroleum inclusions were obtained from microthermometric measurements (Fig. 5). Figure 5 shows that the primary oil inclusions aligned in the rims of dolospars give the highest temperature of 125 °C (Table 1). The hydrocarbon mixtures included all three phases: vapor bubble, liquid oil, and water. The real oil sample is of an orange brown color, and the inclusion shown in Fig. 8b has a width of 150 µm.

Gas-to-oil ratio (GOR)

The phase rule for equilibrium conditions is expressed as follows (Gibbs 1961; England et al. 1987; Atkins and De Paula 2006):

$$P = C - F + 2 \quad (1)$$

where P is the number of phases, C is the number of components, and F is the number of degrees of freedom (generally $F \leq 3$). Under normal subsurface and surface conditions, there are typically three phases in equilibrium: a gaseous petroleum phase, a water phase with minor amounts of hydrocarbon, and a petroleum-rich liquid phase. The solubility of the most hydrocarbon components in water is very low, so the petroleum mixtures are often defined as saturated phases with respect to water.

The GOR at room temperature is a good indicator of the light components fraction in a petroleum inclusion. Based on GOR values at laboratory and subsurface conditions, one can describe the evolution of a hydrocarbon mixture from source rock to reservoir, which holds the mature hydrocarbons available for production. Various experimental, empirical, and theoretical methods have been proposed for GOR calculation (Aplin et al. 1999; Tseng and Pottorf 2002). Some of these methods are based on a measure of the gas bubble filling degree at ambient temperature (Thiéry et al. 2002) as measured by CSLM (Pironon et al. 1998) or by simple visual estimation, as used by Chen et al. (2003) and Benchilla et al. (2003). However, determination of the phase diagram and the PT isochore for petroleum inclusions remains a contentious process (Pironon et al. 1998; Thiéry et al. 2002). It should be noted here that GOR is a dimensionless parameter (kg-gas/kg-oil), and during the course of this research works, it was calculated by using a software for the oil inclusions. GOR also was measured by laser microscopy method and expressed again as a kg-gas/kg-oil for the oil inclusions. For the oil inclusions, the GOR was measured at saturation (homogenization) temperatures. GOR for reservoir oil is expressed as SCF/STBO—Standard Cubic Feet/Stock Tank Barrels Oil—both at same standard conditions.

For the purpose of this study, a confocal laser scanning microscope (Fig. 9) was used to determine F_V of the petroleum inclusions in carbonates samples from Asmari formation at the Kuh-e-Mond (Fig. 10a). The vapor volume percentage measured for the petroleum inclusions was about 4 %, and the T_H value for the inclusion case was determined to be 54 °C (Fig. 10b).

Compositional history and PVT

Migration behavior of a petroleum mixture is a function of petrophysical properties of the target sediment like porosity (φ) and permeability (K) and physical properties of the fluid such as density (ρ) and viscosity (μ) (Danesh 1998; Pedersen and Christensen 2006). The density contrast between the oil and water is the main driving force for migration (buoyancy) as it influences the direction and

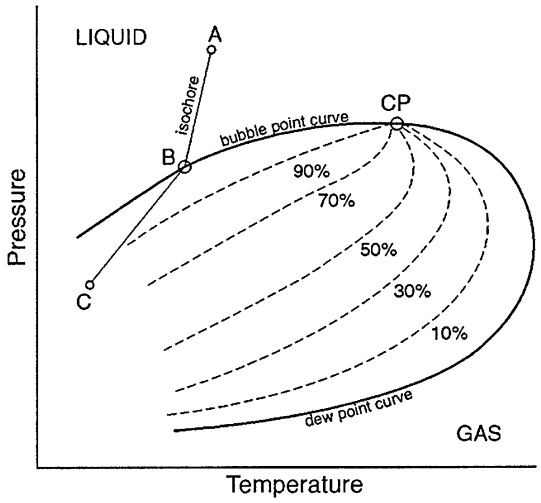

Fig. 7 A typical PT phase diagram of a multi-component mixture

flow rate of the petroleum fluid. According to the Darcy's law, the volumetric flux is inversely proportional to fluid viscosity. Density and viscosity depend on pressure, temperature, and also mixture composition. Characterization of petroleum fluids requires specifying the mixture composition using PVT simulators. In addition, some important parameters such as GOR, molar volume fractions, saturation pressures, component densities, and compressibility factors (Z) are needed to determine the phase envelopes for the petroleum mixtures.

Thermodynamic behavior and evolution of the hydrocarbons mixture during the migration period based on experimental PVT results and microthermometric data of Kuh-e-Mond oil field are presented in Figs. 11 and 12. The liquid–gas immiscibility plot in Fig. 11 is divided by the bubble-point curve and the dew-point curve for a particular petroleum inclusion. The dashed–dotted curves in Fig. 11 are the iso-curves of constant volumetric fraction of the vapor phase. Internal thermodynamic properties such as trapping pressure and temperature of the petroleum inclusions were calculated using volumetric data as shown for the points A, B, and C in Fig. 12.

The flash technique (Aplin et al. 1999; Tseng and Pottorf 2002) was used in this research work to determine the mixture composition and the ratio of gas volume to liquid volume under standard conditions. The mole percent of all liquid and gas components as well as overall composition of the initial mixture is tabulated in Table 2. The GOR was determined to be 0.3 SCF/STBO at surface *P* and *T*.

A PVT simulator is a thermodynamic module that can predict physical properties and composition of the petroleum (e.g., molar fractions of C_{12+} and compositions for liquid and gas phases) trapped inside fluid inclusions. Compositions of the petroleum inclusions of the Kuh-e-Mond oil field obtained from the simulation runs are presented in Table 3. The black-oil PVT simulator is able to calculate the trapping pressure of the inclusions to obtain the composition with the same volumetric fraction at the saturation temperature. The molar fraction of the C_{12+} component was calculated through a seven-step separator using the input data. The final compositions of the multistage separation are reported in Tables 2 and 3. Mole fractions in gas and liquid phases were obtained when thermodynamic equilibrium was established. The PVT simulator determines PT phase behavior, isochrones, and viscosity of the petroleum inclusions (see Table 3). It should be noted here that the flash process was carried out at constant volume of the petroleum mixture in both atmospheric conditions and at the homogenization temperature. The mole fractions of the petroleum inclusions obtained from the simulator are presented in Table 3. A modified Peng–Robinson equation of state (EOS) was used in the PVT simulation software to match the

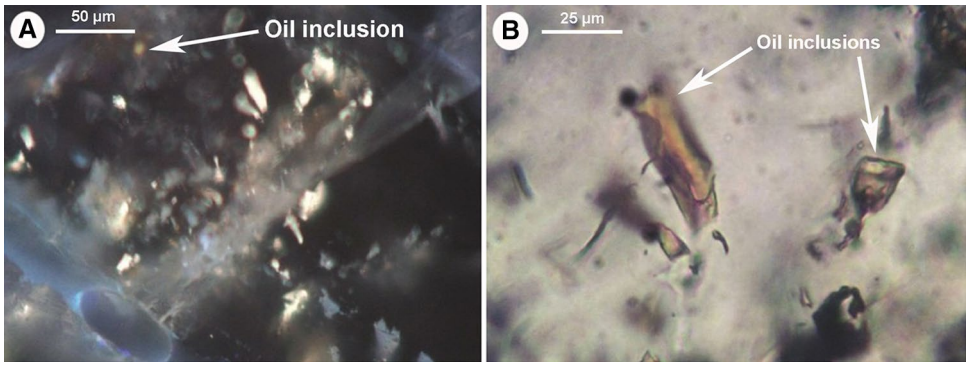

Fig. 8 Photomicrographs of oil inclusions in doubly polished wafers; **a** a view of the oil inclusions under incident UV (width of view: 300 µm); **b** larger image of the inclusions in part using transmitted light. The real oil sample is of an orange brown color and the inclusion (**b**) has a width of 150 µm

thermodynamic behavior of the petroleum mixture (Peng and Robinson 1976).

The main steps to run the PVT simulation software are summarized briefly as the following:

Step 1 Select the composition of the initial mixture
Step 2 Use a PVT simulator to calculate the saturation pressure of the petroleum inclusions at saturation temperature (homogenization temperature)
Step 3 Perform a flash process to compute the mixture composition at the homogenization temperature and saturation pressure
Step 4 Calculate the saturation pressure of the original mixture at room conditions. Since the petroleum mixture has two phases based on thermodynamic condition, the saturation pressure is the maximum possible pressure for the inclusion
Step 5 Do a series of flash (vapor/liquid equilibrium) calculations at room P and T below the saturation pressure
Step 6 Calculate the GOR of the original petroleum inclusion at room temperature and the internal pressure. If the calculated GOR matches the measured one using the CLSM techniques, the composition of the petroleum inclusion was selected accurately and the petroleum inclusion used for the simulation modeling is a good representative of the real mixture
Step 7 If the difference between the calculated GOR and the measured GOR is relatively high, gas titration will be done on the initial mixture, and the entire procedure will be repeated until convergence is achieved.

The molar compositions obtained from the PVT simulator are usually expressed in terms of carbon number fraction as reported by Katz and Firoozabadi (1978). A carbon number fraction consists of all components with boiling points higher than that of the n-alkane with $(n-1)$ carbon atoms and less than or equal to that of the n-alkane with n carbon atoms. The standard molar composition for the oil inclusion used in the PVT calculations is presented in Table 4. The accuracy of the calculation strongly depends on the experimental work, which was carried out to obtain trapping parameters (e.g., Th) and the volumetric data. Experimental data and simulation results for the single-stage separator are also presented in Table 4. In addition, the molar flow rates of the gas and liquid phases, saturation pressure, and other system properties at different thermodynamic conditions are also tabulated in Table 4 for the oil samples from the Kuh-e-Mond heavy oil field. It should be noted here that the properties of the oil inclusions with $T_H < 60$ °C are calculated at 15 °C and 1 bar (100 kPa). Pressure and temperature of the petroleum mixture were estimated at 79 bar (7,900 kPa) and 54 °C during the migration event, respectively. The vapor volumetric percent and GOR were also determined to be 4 % and 4 kg-gas/kg-oil at standard conditions, respectively.

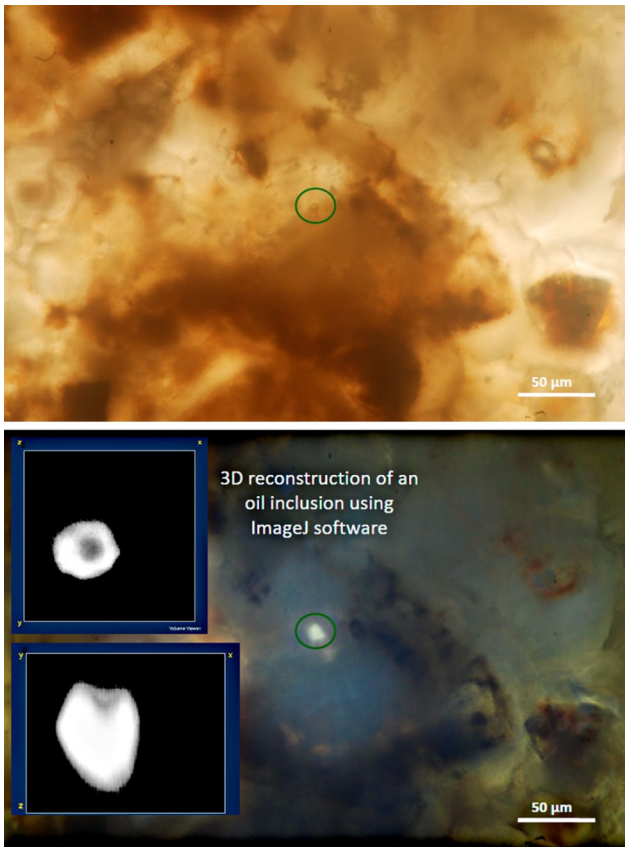

Fig. 9 CLSM–GOCAD 3D image of a petroleum inclusion sample taken from the Asmari formation at Kuh-e-Mond

Discussion

In this section, results obtained from different parts of this research work are discussed. Various techniques are used, and several parameters are determined to reconstruct the charge history and characterize the PVTX behavior of the Kuh-e-Mond heavy oil field. At the end, significance of the finding of this research is further delineated, and its possible implications are discussed, briefly. In addition, some future research works and research objectives are suggested on the basis of current work.

Microthermometry

Most of the primary oil inclusions in the early equant calcite cement were homogenized between 51 and 56 °C (Sample zsh4 in Table 1). Aqueous types were precipitated at temperatures above 35 °C in the presence of

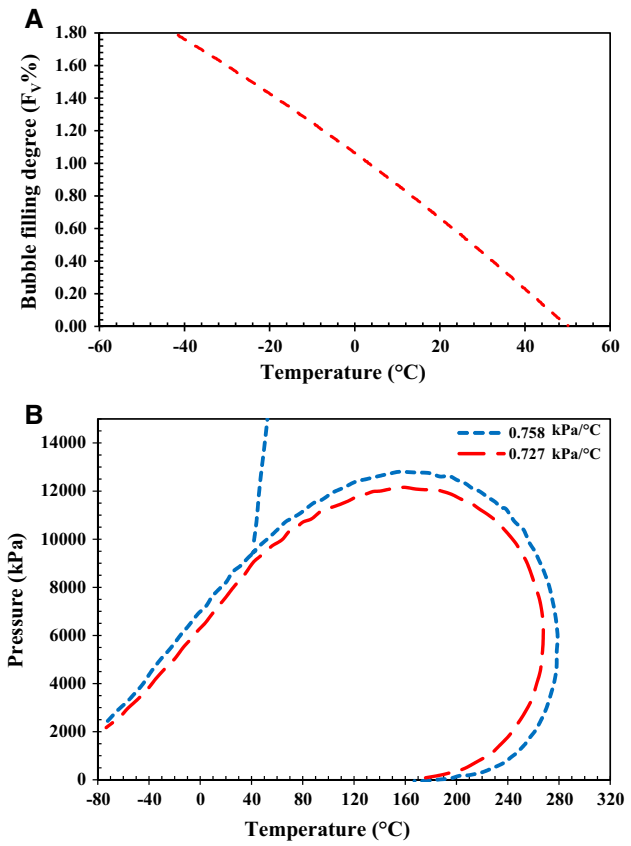

Fig. 10 **a** Bubble filling degree (F_V %) at different temperatures for an oil inclusion from the Kuh-e-Mond measured by confocal laser scanning microscopy. In this case, the T_H is 54 °C. **b** PT phase envelope for two different petroleum inclusions with T_H of 53 and 100 °C calculated from the molar composition of the inclusions. The slopes of the isochores are 0.726 and 0.758 kPa/°C. Projection of the isochores at present reservoir temperature gives pressures not higher than 120 bar. This indicates that the rate of pressure increase in this reservoir has been very slow since the inclusions were trapped. Present-day low pressure at the reservoir also confirms this

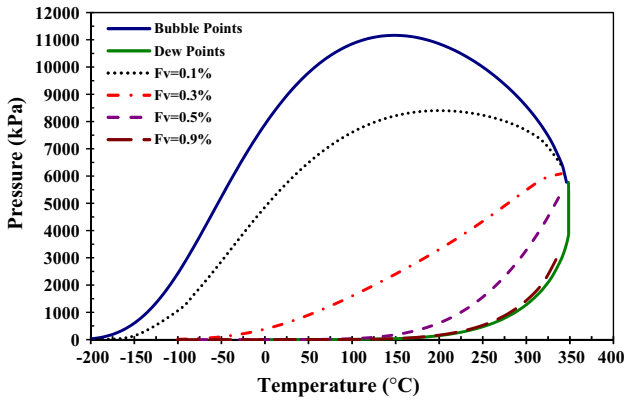

Fig. 11 PT phase diagram of a petroleum inclusion based on the microthermometric data

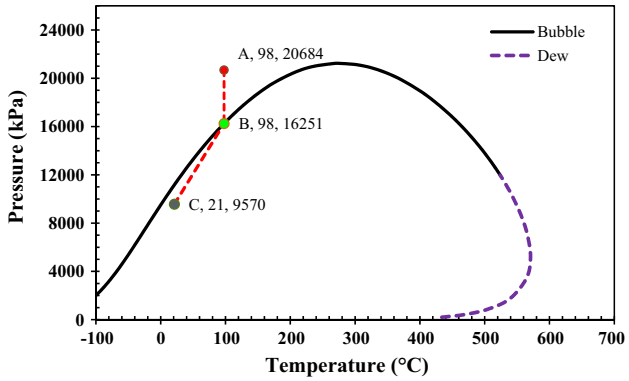

Fig. 12 PT pathway of the hydrocarbon inclusion shown on the PT envelope

high salinity fluids (~22 eq. wt% NaCl) (Sample zsh4 in Table 1). This was followed by precipitation of coarser sparry calcite cement fracture/vein fillings formed at temperatures largely above 55 °C to at least 85 °C based on the temperature data from primary aqueous inclusions. Fluids were of high salinity (ca. 19–22 eq. wt% NaCl), and they were more saline in the equant calcite case (Sample zsh12 in Table 1). Consequently, the equant calcite was formed at lower temperatures than the coarse vein-filling calcite cements, which predate the petroleum emplacement. This means that the equant calcite is a depositional texture and does not contain oil inclusions. The dolospars revealed precipitation temperatures (representing the outer dolomite rims) above 65 °C continuing to at least 125 °C (Sample zsh23 in Table 1). The dolomite phase (cement rims on dolospars even in upper parts of reservoir) postdates calcite vein cements with highest temperatures, which is consistent with the highest calcite temperatures (65–85 °C) in the entire reservoir. Salinities were approximately 19 eq. wt% NaCl. Furthermore, oil was present during calcite precipitation in the fracture/vein. T_H values of the oil inclusions (51–56 °C) were higher in sparry calcite compared to anhydrite laths demonstrating relative cooling (Table 1). The measured T_H values of oil inclusions (ca. 22–47 °C) are much lower than those of aqueous inclusions in the vein-filling calcite. This indicates significant undersaturation with respect to gas. T_H (beginning at 35 °C) increases during precipitation of various calcite cement phases from early equant (>35 and <45 °C) toward the fossil cavities (>45 °C). The granular calcite mosaic crystals and sparry vein-filling phases have T_H about 80–98 °C (>70 °C), which is an indication of salinity of ca. 18–22 eq. wt% NaCl (the brines were migrating along with hydrocarbon). As can be seen from Fig. 6, the T_H evolution from equant toward vein fill calcite corresponds to early and shallow burial cementation and an influx of water with different

Table 2 Compositions of gas, liquid, and original mixture of the reservoir hydrocarbons (oil)

Components	Flashed oil (mol%)	Flashed gas (mol%)	Subsurface reservoir oil (mol%)
H_2S	0	0	0
N_2	0	3.68	0.66
CO_2	0	1.28	0.23
C_1	0	58.03	10.35
C_2	0.12	12.62	2.35
C_3	0.42	8.98	1.95
iC_4	1.53	2.06	1.62
nC_4	3.76	5.11	4
iC_5	3.95	1.95	3.6
nC_5	2.31	2.14	2.28
C_6	2.85	2.23	2.74
C_7	2.33	1.33	2.15
C_8	2.83	0.53	2.42
C_9	2.6	0.07	2.15
C_{10}	3.81	0	3.13
C_{11}	3.07	0	2.52
C_{12+}	70.42	0	57.86
GOR: 75.21 SCF/STBO	Total: 100	Total: 100	Total: 100

Table 3 Compositions of the oil inclusions from Kuh-e-Mond obtained from simulation runs

Components	Mole%
H_2S	0
Nitrogen	4.020
CO_2	0.295
C_1	4.175
C_2	2.500
C_3	1.720
i-C_4	1.350
n-C_5	3.300
i-C_5	2.920
n-C_5	1.840
n-C_6	2.200
n-C_7	1.720
n-C_8	1.940
n-C_9	1.720
n-C_{10}	2.500
n-C_{11}	2.020
n-C_{12}	2
n-C_{12+}	46.284

Compositions of petroleum fluid inclusions calculated at 97.7 °C

composition during burial with lower salinity during cooling. Primary aqueous inclusions with salinity of 20.5 eq. wt% NaCl for anhydrite laths demonstrate T_H values considerably less than values reported from primary aqueous inclusions in the calcite cements.

The occurrence of the monophase inclusions indicates that anhydrite was formed at lower temperatures under a phase of cooling between precipitations of the two minerals. However, except for the inclusions found in the calcite cements at the base of the Asmari formation, the upper Asmari vein-filling dolomite displays the highest T_H values confirming dolomite precipitation temperatures above 85 °C possibly to at least 105 °C (Max. 125 °C). The estimated water salinities are also 19.8–21.3 eq. wt% NaCl (~5 times more saline than seawater). The recorded range of salinities should record a transition from marine to higher salinity waters. Oil was present during calcite (27–65 °C)/dolomite (68–104 °C)/anhydrites (47–46 °C) precipitation in the fractures and veins (Table 1). The oil inclusion data also suggest that the onset of carbonate cementation occurred at temperatures above 45 °C and that cementation was progressive through burial and diagenesis. The cementation event is concurrent with early petroleum generation and migration because saline waters were trapped in some oil inclusions. Based on the T_H data, it can be concluded that the pore fluids became warmer and more saline during burial as would be expected with increasing depth. The lower T_H ranges for anhydrite suggests its occurrence at shallower burial depths. A distinctive rise in the T_H values from equant to vein calcite recognizes a change in water composition. Calcite and dolomite vein fills associated with oil inclusions cements were precipitated from petroleum-derived fluids as well. The oil inclusions within the vein-filling sparry calcite cements had a T_H value of 51–85 °C (Table 1), which demonstrates a relative cooling behavior. A high T_H indicates late migration of moderately less undersaturated oil in the reservoir.

PVT simulation

T_H and F_V of the two-phase petroleum inclusions were calculated using experimental work and simulation as shown in Fig. 10a, b. The lowest T_H and F_V values represent the oil mixtures with the highest densities. After adding 0.2 mol of methane to the oil inclusion, the characteristics of the new petroleum fluid were calculated using correspondent T_H and F_V (see Fig. 10a). Results obtained from the PVT black-oil simulator indicate that the reservoir pressure and temperature were set at 100 bar (10,000 kPa) and 54 °C during the initial stages of oil migration and even an increase in the amount of gas phase had no considerable effect on reservoir pressure.

Table 4 Characteristics of the oil inclusions obtained from PVT simulation

Stream name	16
Vapor/phase fraction	1.95E−02
Temperature (°C)	15
Pressure (kPa)	7,900
Molar flow (kg mole/h)	125
Mass flow (kg/h)	13,286.98
Std ideal liqvol flow (m^3/h)	19.20728
Molar enthalpy (kJ/kg mole)	−234,437
Molar entropy (kJ/kg mole °C)	191.8402
Heat flow (kJ/h)	−2.9E+07
Liqvol flow @std cond (m^3/h)	18.75555
Fluid package	Basis-1

The last oil inclusion has the heaviest components as the mole fractions of C_{12} and C_{12+} are 0.46 and above 0.40, respectively (Table 3). The amounts of light components such C_2 and C_3 are also very small in the oil mixture. Mole fractions of methane and nitrogen in the gas phase decrease as the number of stages increases, based on the composition of the mixture exiting from the multistage separator. However, the mole fractions of other gaseous components increase with increase in the number of flash separators (Fig. 13). Also, it can be concluded here that a gas phase with higher density was obtained in the last stage of the flash processes as the specific gravity of the gas phase at the first stage was about 0.7, but it reaches 1.25 at the last flash stage.

The highest methane content was also reported around 21 wt% at an average T_H of 54 °C. The *P*–*T* conditions of fluid inclusion entrapment determined using a PVT black-oil simulator are shown in Fig. 10b. An increase in temperature of the trapped petroleum causes an increase in the mixture pressure and also an increase in the saturation pressure, as shown in Fig. 10a. The releasing temperature during petroleum fluids mixture upwelling from a greater burial depth to a shallower condition leads to some geochemical reactions and precipitation of carbonate cements in the open spaces.

The petroleum compositions modeled here (See Table 3) indicate a satisfactory agreement between the experimental data and the simulation outputs. Based on mole fractions of C_1 and C_2 in Tables 2 and 3, it can be also concluded that primary and secondary cracking in the source rocks were responsible for retention of heavy components and migration of miscible three-phase flow during hydrocarbon evolution. According to GOR contours variations at surface condition, oil and gas densities increase by increase in mixture pressure but decrease slightly if the temperature increases (Fig. 10b). The most important feature of the petroleum liquid is that the subsurface density decreases with increase in pressure. However, the subsurface gas density behaves in a completely different way. Density increases with increase in pressure similar to the normal PVT behavior of gases. The simulation results showed that the gas density reaches about half of the liquid petroleum at pressure of 80 bar (8,000 kPa).

The molar distributions were regressed to obtain the dew-point, bubble-point, and critical point values, based on the mole percent and the molecular weight of the plus fraction in the petroleum inclusion as shown in Fig. 11. Hence, using standard molar compositions in PVT computations generates results with high accuracy (see Table 4). If standard compositions are used in the simulation runs, then the predictions are generally better than those based on extended molar compositions. The amount of lighter hydrocarbons in the petroleum mixture significantly affects the subsurface composition and GOR values. In addition, these values can vary during oil migration due to different processes involved such as liquid–gas unmixing, hydrocarbon mixing, leaching by a gas phase or an aqueous solution, biodegradation, and gravity segregation (Taylor et al. 1997; Larter et al. 2000). All of these processes can be identified in oil-bearing petroleum inclusions as they entrap consecutive aliquots of migrating or charging fluids. After fluid entrapment, other phenomena such as leakage, necking down, chemical reactions, decrepitation, and implosion can also change the characteristics of the oil inclusions (Bodnar 1993). Hence, it is usual to observe very different ($F_V - T_H$) behaviors in some series of petroleum inclusions in the same sample.

Changes in oil pressure and/or temperature generally happen during the evolution of oil field. Pressure changes can take place, for instance, when fractures are opened because of the overpressure applied by petroleum mixtures causing a significant reduction in fluid pressure. Burial of a reservoir or its uplift can also result in instantaneous *P* and *T* changes. Any petroleum inclusions later trapped will have the same composition as those trapped earlier in case pressure reduction is not enough to make a liquid–gas unmixing (England et al. 1987; Goldstein and Reynolds 1998; Kamali and Rezaee 2003). Saturation pressure as a function of C_1 mol% is presented in Fig. 14. Saturation pressure varies between 50 bar (5,000 kPa) and 500 bar (50,000 kPa). The T_H is in the range of 30–130 °C, hence covering the typical range of homogenization temperatures of fluid inclusions. As shown in Fig. 14, if the concentration of CH_4 in the hydrocarbon mixture increases, then saturation pressure will increase so that the highest saturation pressure (470 bar or 47,000 kPa) corresponds to the greatest mole percentage of C_1 which is 85 % in the last stage of flash.

The PT conditions of the fluid inclusion entrapment determined using a PVT black-oil simulator are presented in Fig. 15. The pressure evolution depicted in Fig. 15 clearly shows that mixture pressure (consequently, the

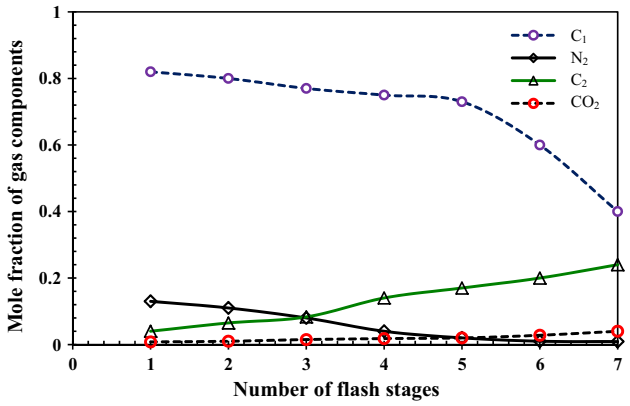

Fig. 13 Mole fraction of gas components at various flash separators

saturation pressure) increases as the temperature of the trapped petroleum increases. The main reasons for increase in temperature could be geochemical reactions during petroleum migration or/and the mixture being stored at greater depths (greater burial depth). Exothermic processes that generate heat normally occur in oxidation–reduction reactions, which take place by respiring and anoxygenic photosynthesis microorganisms. For example, during generation of methane by bacteria, hydrogen reduces carbon dioxide and sulfur and the consequent hydrogenation of the petroleum hydrocarbon components releases heat. Also, during metabolic activities of microorganisms, reactions between acetylene and water releases methane generate heat (MacGregor and Keeney 1973; Song et al. 2004).

The geochemistry and PVT outcomes of this research work support the scenario of uplifting the Kuh-e-Mond anticline during and after oil migration, which caused rapid segregation of the oil mixture in the reservoir. The segregation phenomenon generally happens after high PT conditions that change the conditions to non-equilibrium status and also make gases to escape from the mixture. This process is facilitated by presence of vertical and sub-vertical fractures in the carbonate strata.

Petroleum inclusion samples that have F_V values consistent with present-day trapping within the oil reservoir were selected to examine the precision of the PVT simulation. The results show that the PVT simulations calculate fluid properties of the oil inclusions with a high accuracy and a relatively low absolute error percentage of less than 10 %. PVT analysis of the petroleum inclusions from Asmari reservoir at the Kuh-e-Mond oil field confirms that variations in the oil composition occurred along the migration pathway are consequences of gradual displacement of the earlier stored oil by later migrated gas. This demonstrates potential value of petroleum inclusion technology in assessment of oil quality, migration time period, entrapment history, and in limiting the outputs of formation modeling.

Implications

Heavy oil is almost always biodegraded light oil. Light oil travelled upward through buoyancy and laterally through advective flowover long distances from deep source rocks (>3,000 m deep) to shallower strata. There, the oil was exposed to bacteria (biodegradation), different groundwater chemistry, more rapid groundwater flux (water washing), and reduced pressure (causing loss of light molecules through diffusional processes). Biodegradation is controlled mainly by temperature, chemical composition of the oil and groundwater, and the relation between the oil volume and the oil–water contact area. Biodegradation affects petroleum fluid properties (lowers the API gravity and increases the in situ viscosity of the oil), alters the oil geochemistry, and increases the asphaltene content, sulfur content, acidity, and concentration of heavy metals in the oil (Head et al. 2006; Larter et al. 2006; Eschard and Huc 2008). Gradients in oil composition and viscosity variations are common at reservoir scales both vertically and horizontally and are linked with proximity to active water (slow flux) and geochemical factors. As an example, researchers studied the organic geochemistry of oil inclusions from heavy oil reservoirs in Oman, also occurred in naturally fractured carbonates as a close analogue to the Kuh-e-Mond heavy oil field, and reported that water washing caused removal of light components ($<C_{12}$) from the petroleum fluids (Burrus et al. 1985; Mauk and Burruss 2002). Changes from biodegradation, water washing, and evaporation of the light hydrocarbons are known as post-generation alteration (Canipa-Morales et al. 2003; Mango 1997). This scenario is valid for the majority of the known heavy oil accumulations in the world such as Canadian and Venezuelan oil sands, as well. The standard scenario for generation of heavy oil as described earlier in this section (Fig. 16) is primarily developed for oil sands, but it is also valid for heavy oil deposits found in naturally fractured carbonate rocks. However, further research is needed to determine the origin of the heavy oil in the Middle East, mostly found in deep naturally fractured carbonate heavy oil reservoirs (Dusseault and Shafiei 2011). The presence of fractures and also differences in chemistry of the reservoir rocks and also the formation water can affect heavy oil generation processes in this type of reservoirs.

The Iranian heavy oil deposits, including the Kuh-e-Mond heavy oil field, are mainly biodegraded light oil originating from different organic rich shale units in the region. After sedimentation, burial and generation of oil in the Persian Gulf oil system (Zagros Foreland Basin) and subsequent tectonic activities caused vertical and up-dip migration of the oil in naturally fractured carbonate rocks into a shallower depth through fracture systems. Subsequent biodegradation, water washing, and some other processes

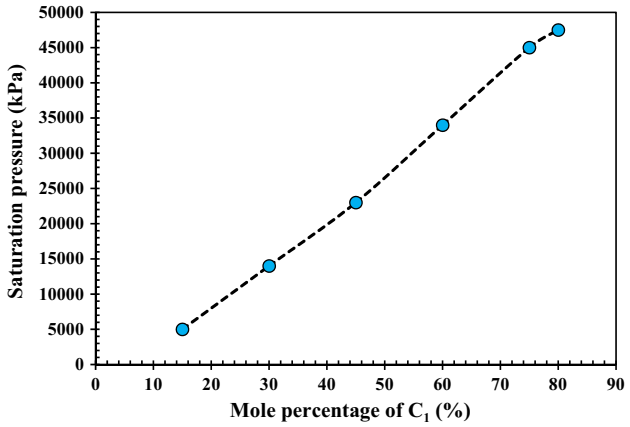

Fig. 14 Saturation pressure versus mole percentage of methane in the petroleum inclusions

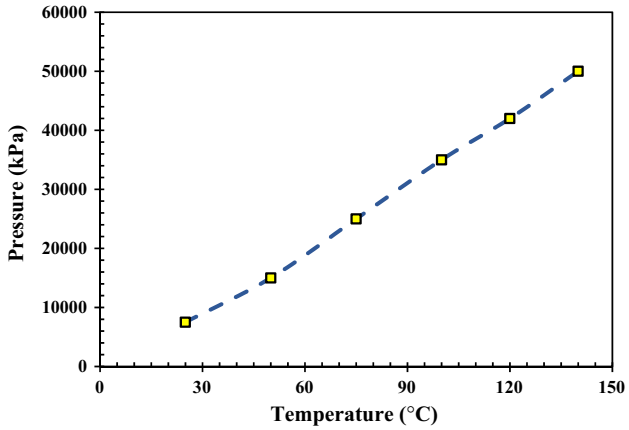

Fig. 15 Pressure evolution of the oil inclusions during the migration event

transformed the light oil into heavy oil. Furthermore, ongoing tectonic activities after formation of heavy oil in the Zagros Foreland Basin led to more folding and fracturing and in some cases additional burial. This scenario explains the existence of some heavy oil deposits found at depths greater than 3,000 m (4,000–4,300 m in one case). Such a depth is beyond the reach of biological activities, which are essential in formation of heavy oil. In the case of the Kuh-e-Mond field, a network of extensive vertical and subvertical fractures as well as permeable horizontal bedding planes allowed groundwater recharging into the heavy oil field leading to oxygen breakthrough to primary unaltered hydrocarbons. This scenario supports that water-washing processes affect generation of heavy oil in the reservoir as well. Study of some analogue heavy oil fields in the Middle East such as heavy oil fields in Oman also supports this scenario. The geology of the study area confirms biodegradation during heavy oil formation, but further research is required to determine the origin of the light oil, and the weighting of different processes involved in generation of heavy oil found in this field such as biodegradation, water washing, cracking, and fractionation. To help determine the origin of heavy oil at Kuh-e-Mond, a viscosity gradient model should be incorporated in composition simulations using Toil and Boil approach to define the extent of the biodegradation. For more accurate results, using a series of biomarker parameters of fluid inclusion oils is also required to assess fractionation and maturation of the petroleum fluids in the region (Thompson 1979, 1983, 1987, 1988).

The main focus of this research work was on delineation and understanding of thermodynamic conditions, physical properties, and composition of the heavy oil in the Kuh-e-Mond heavy oil field in Iran. These factors are considered as key parameters to understand processes (e.g., biodegradation), which led to formation of such heavy oil deposits. One of the main implications of this research on heavy oilfields is that by linking petroleum geochemistry data to modeling simulation, the characteristics of the petroleum can be defined, and it is possible to track systematic variations and changes in fluid properties caused by post-entrapment alterations to predict production fluid molecular compositions over short distances in the reservoirs (Larter et al. 2008). The literature in this area yields little data published on determining thermodynamic conditions, physical properties, and composition of heavy oil, extra heavy oil, and bitumen that occur in naturally fractured carbonate rocks such as the ones reported in the Middle East, and bitumen saturated Devonian carbonates in Alberta, Canada. Despite differences in geological settings and occurrence of heavy oil, extra heavy oil, and bitumen deposits in carbonate rocks around the world, the experimental and simulation data generated here can be beneficial to other researchers by delimiting fluid properties and furthering understanding of different processes and their relative weights in genesis and occurrence of heavy oil, extra heavy oil, and bitumen deposits in carbonate rocks. In the case of the Middle East, given the significant similarity in geological setting and physical and chemical properties of the petroleum fluids, data and findings presented in this study can be used as an analogue for similar heavy oil reservoirs in the region such as the ones reported in Oman and Kuwait.

Conclusions

Microthermometry and PVTX laboratory experiments and simulations were used to determine thermodynamic conditions, physical properties, and composition of heavy oil samples from the Asmari formation reservoir, which forms part of the Kuh-e-Mond heavy oil field in Iran. The following main conclusions can be drawn based on the results of this study:

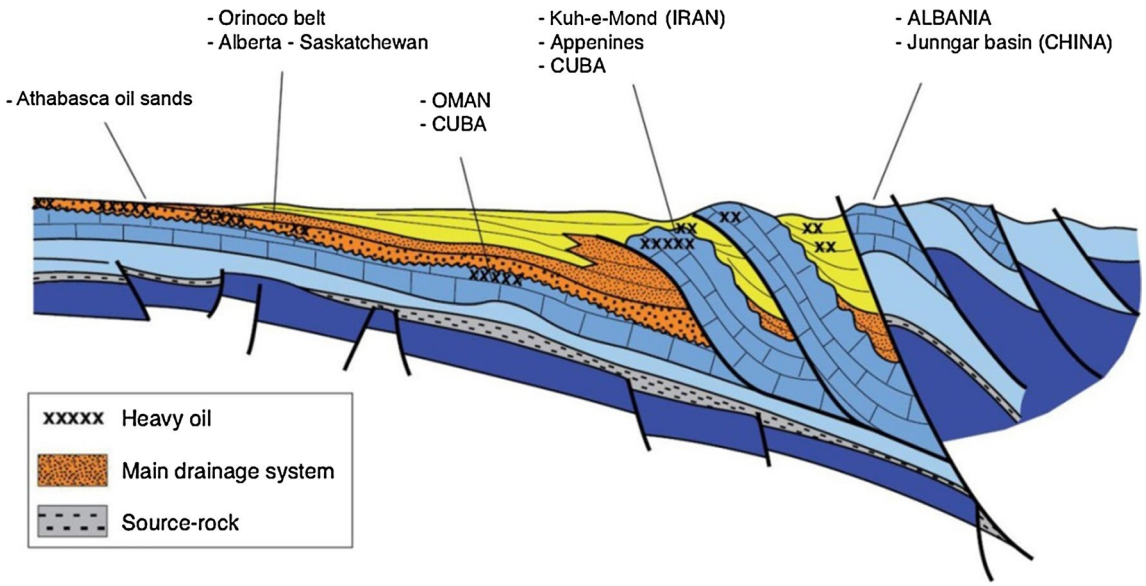

Fig. 16 A basin-tectonic context for naturally fractured carbonate heavy oil deposits [modified from Eschard and Huc (2008)]

1. Microthermometry results indicate that the equant calcite was formed at lower temperatures than the coarse vein-filling calcite cements, which predates petroleum emplacement (primary in terms of origin). Microthermometry technique proved useful in interpreting fluid inclusion assemblages as both primary (isolated or along growth zones) and secondary (trapped along fracture and cleavage planes).
2. Based on the oil inclusion data, the onset of carbonate cementation occurred at temperatures above 45 °C, and it progressed through burial diagenesis.
3. PVT black-oil simulator results suggest that the reservoir pressure and temperature were set at 100 bar and 54 °C during the initial stages of oil migration. This knowledge can be used to understand the level and extent of other factors contributing to generation of heavy oil in the study area.
4. Based on the mixture composition from the multistage separator, there is a decrease in mole fractions of CH_4 and N_2 in the gas phase with increase in the number of stages. Understanding the evolution of composition of the petroleum fluids can shed light on determining the different stages the petroleum fluids has undergone.
5. According to GOR contour variations at surface conditions, oil and gas densities increase as the mixture pressure increases and decrease slightly as the temperature increases.
6. The PT evolution of petroleum inclusions indicates that PVT properties and mobility changes due to phenomena such as cracking, mixing, or transport took place at various stages of oil migration to the reservoir.
7. Compositional modeling showed that primary and secondary cracking in source rocks were responsible for retention of heavy components and migration of miscible three-phase flow during the hydrocarbon evolution.

Acknowledgments The authors would like to thank Dr. Fran Hein (ERCB, Calgary, AB, Canada), Dr. Philipp Kuhn (Shell, Netherlands) and Dr. Jürgen Grötsch (Shell, Netherlands), topic editor of the IJES, for their critical but fair review of the manuscript which improved the quality and clarity of the manuscript. The authors also wish to thank Prof. Régis Thiéry (Blaise Pascal University, France), Dr. Nafiseh Farhadian (Ferdowsi University of Mashhad, Iran) and Prof. Maurice B. Dusseault (University of Waterloo, Canada) for their useful review and comments on an earlier draft of this manuscript.

Appendix: Equations and software procedures

The generalized properties of petroleum phases and water are affected by pressure, temperature, and composition (PTX) and were calculated by using correlations and thermodynamic calculations explained here. The correlations are based on laboratory experiments (e.g., Standing 1952; Glasø 1980) and are accurate enough for the purposes of this study. In addition, these have been validated by process and plant engineers. In these equations, the following dependence of the mole fraction on carbon number is assumed:

$$Z_n = \exp(A + BC_n) \quad (2)$$

where Z_n is the total mole fraction of the components with C_n carbon atoms, and A and B are constants. It has previously been shown that these distribution functions can be

used to represent reservoir fluid compositions to at least C_{19} (Pedersen et al. 1984). The compositions of petroleum reservoir fluids are most often reported to C_{7+}, C_{10+}, or C_{20+} and in rare cases to C_{30+} (Katz and Firoozabadi 1978; Pedersen et al. 1989).

Simulators of petroleum use minimum compositional data which are the mole percent of C_1–C_6 alkanes and isoalkanes, inorganic gases plus a single value for C_{7+}; determine PT phase behavior, phase diagram, isochores, viscosity, and GOR (GOR = C_1–C_5/C_{6+}). The molar compositions of the reservoir fluids are determined from compositional analyses of the gas and liquid phases resulting from a flash of the reservoir fluid to STP conditions of 15 °C and 0 bar (Fig. 14). The simulator is dealing with multi-component hydrocarbon system and mole fraction (*x*,*y* factor) of the inclusions along with the liquid: vapor ratio, GOR, viscosity, molar volume, density, surface tension, and physical parameters such as formation volume factor, solubility, viscosity, compressibility factor (*Z* factor), density, solubility, and formation volume factor, which are all necessary for black-oil flow simulations as a function of pressure.

Z_i represent the molar distributions of the C_{7+}, fractions in the oil, the coefficient of determination (r^2) has been calculated for each mixture. In Eq. 3, x_i and y_i are paired values of observations and n is the number of observations:

$$r^2 = \frac{\left[\sum \dot{x}_i \ln y_i - {}^1\!/_n \sum x_i \sum \ln y_i\right]^2}{\left[\sum x_i^2 - \frac{(\sum x_i)^2}{n}\right]\left[\sum (\ln y_i)^2 - \frac{(\sum x_i)^2}{n}\right]} \quad (3)$$

Assuming the distribution function of Eq. 2, x_i, and y_i are corresponding values of carbon number and mole fraction. The value of r^2 lies between 0 and 1 and will indicate how closely the equation considered fits the experimental data. The closer the P is to 1, the better the fit. The final values for P for each of the oil mixtures are shown in Table VI of Pedersen et al. (1989). The average value of 1.2 obtained using the distribution function of Eq. 2 is 0.9815. This is very close to 1, and it can therefore be concluded that Eq. 2 represents the experimental molar distributions, reasonably.

PVT calculations

Various PVT properties have been measured for the reservoir fluids in this study. In order to investigate how closely the measured PVT properties can be predicted using standard molar compositions and extended molar compositions, the SRK equation in the modified form proposed by Peneloux et al. (1982) was used. The critical P and T and the acentric factors of the C_{7+} fractions were calculated using the following relations (Pedersen et al. 1989):

$$T_c = c_1\rho + c_2 \ln MW + c_3 MW + c_4/MW \quad (4)$$

$$P_c = d_1\rho + d_2\rho = d_3/MW + d_4/MW^2 \quad (5)$$

$$M = e_1\rho + e_2 MW + e_3\rho + e_4 MW^2 \quad (6)$$

where the values of the coefficients c_1–c_4, d_1, d_4, and e_1–e_4 are given in Table VII of Pedersen et al. (1989), and m is a function of the acentric factor ω as the following:

$$m = 0.480 + 1.574\omega - 0.17\omega^2 \quad (7)$$

The densities used in Eqs. 4–6 were estimated using a methodology described by Pedersen et al. (1984). The molecular weights were also determined from Eq. 4.

References

Adams J, Riediger C, Fowler M, Larter SR (2006) Thermal controls on biodegradation around the Peace River tar sands: paleo-pasteurization to the west. J Geochem Explor 89:1–4

Ahmadhadi F, Lacombe O, Daniel JM (2007) Early reactivation of basement faults in Central Zagros (SW Iran): evidence from pre-folding fracture populations in Asmari Formation and lower Tertiary paleogeography. In: Lacombe O, Lave´ J, Roure F, Verges J (eds) Thrust belts and foreland basins from fold kinematics to hydrocarbon systems. Springer, Berlin, pp 205–228

Aplin AC, Macleod G, Larter SR, Pedersen KS, Sorensen H, Booth T (1999) Combined use of confocal laser scanning microscopy and PVT simulation for estimating the composition and physical properties of petroleum in fluid inclusions. Mar Pet Geol 16:97–110

Aplin AC, Larter SC, Bigge MA, Macleod G, Swarbrick RE, Grunberger D (2000) PVTX history of the North Sea's Judy oilfield. J Geochem Explor 69–70:641–644

Atkins PW, De Paula J (2006) Physical chemistry, 8th edn. Oxford University Press, Oxford. ISBN 0198700725. Chapter 6

Bahroudi A, Koyi HA (2004) Tectono-sedimentary framework of the Gachsaran Formation in the Zagros foreland basin. Mar Pet Geol 21:1295–1310

Bakker RJ, Jansen JBH (1990) Preferential water leakage from fluid inclusions by means of mobile dislocations. Nature 345:58–60

Bakker RJ, Jansen JBH (1991) Experimental postentrapment water loss from synthetic CO_2–H_2O inclusions in natural quartz. Geochim Cosmochim Acta 55:2215–2230

Bakker RJ, Jansen JBH (1994) A mechanism for preferential H_2O leakage from fluid inclusions in quartz, based on TEM observations. Contrib Mineral Petrol 116:7–20

Bashari A (1988) Occurrence of heavy crude oil in the Persian Gulf. Paper presented at the Fourth UNITAR/UNDP International Conference on Heavy Crude and Tar Sands Edmonton, AB, Canada, 7–12 August, pp 203–214

Benchilla L, Guilhaumou N, Mougin P, Jaswal T, Roure F (2003) Reconstruction of palaeo-burial history and pore fluid pressure in foothill areas: a sensitivity test in the Hammam Zriba (Tunisia) and Koh-i-Maran (Pakistan) ore deposits. Geofluids 3(2):103–123

Bigge MA, Petch GS, Macleod G, Larter SR, Aplin AC (1995) Quantitative geochemical analysis of petroleum fluid inclusions: problems and developments. In: Grimalt JO, Dorronsoro C (eds) Proceedings 17th international meeting on organic geochemistry. European Association of organic geochemists, San Sebastian, pp 757–7590

Bodnar RJ (1993) Revised equation and table for determining the freezing point depression of H2O-Nacl solutions. Geochim Cosmochim Acta 57(3):683–684

Bodnar RJ (1999) The effect of small (undetectable) amounts of water on pressure determinations from carbon dioxide inclusions (Abstract). ECROFI XV, European conference on research on fluid inclusions XV, Potsdam, Germany, pp 21–24

Bodnar RJ, Bethke PM (1984) Systematica of stretching of fluid inclusions I: fluorite and sphalerite at 1 atmosphere confining pressure. Econ Geol 79:141–161

Bordenave ML, Burwood R (1995) The Albian Kazhdumi Fm of the Dezful Embayment, Iran: one of the most efficient petroleum generating systems. In: Katz BJ (ed) Petroleum source rocks. Case book in earth sciences. Springer, Berlin, pp 183–207

Burrus RC, Cercone KR, Harris PM (1985) Timing of hydrocarbon migration: evidenced from fluid inclusions in calcite cements, tectonics and burial history. In: Carbonate cements. Society of economic paleontologists and mineralogists, Special Publication, Tulsa, no. 36, pp 277–289

Burruss RC (1991) Practical aspects of fluorescence microscopy of petroleum fluid inclusions. In: Barker CE, Kopp OC (eds) SEPM short course, vol 25, pp 1–7

Burruss RC (1992) Phase behavior in petroleum-water (brine) systems applied to fluid inclusion studies (Abstract). In: PACROFI IV, Pan American conference on research on fluid inclusions, Program and abstracts, Lake Arrowhead, Ca, vol 4, pp 116–118

Canipa-Morales NK, Galan-Vidal CA, Guzman-Vega MA (2003) Effect of evaporation on C_7 light hydrocarbon parameters. Org Geochem 34:813–826

Chen H, Wang J, Xie Y, Wang Z (2003) Geothermometry and geobarometry of overpressured environments in Qiongdongnan Basin, South China Sea. Geofluids 3:177–187

Danesh A (1998) PVT and phase behaviour of petroleum reservoir fluids. Elsevier Science, Amsterdam

Di Primio R, Dieckmann V, Mills N (1998) PVT and phase behavior analysis in petroleum exploration. Org Geochem 29(1):207–222

Dubessy J, Buschaert S, Lamb W, Pironon J, Thiery R (2001) Methane-bearing aqueous fluid inclusions: Raman analysis, thermodynamic modeling and application to petroleum basins. Chem Geol 173:193–205

Dusseault MB, Shafiei A (2011) Oil sands. Ullmann's Encyclopedia of chemical engineering. Wiley, London, p 52

England WA (1990) The organic geochemistry of petroleum reservoirs. Org Geochem 16:415–425

England WA, Mackenzie AS, Mann DM, Quigley TM (1987) The movement and entrapment of petroleum in the subsurface. J Geol Soc 144:327–347

England WA, Mann AL, Mann DM (1991) Migration from source to trap. In: Merril RK (ed) Source and migration processes and evaluation techniques. Handbook of petroleum geology. AAPG Bull, pp 23–46

Eschard R, Huc AY (2008) Habitat of biodegraded heavy oils: industrial implications. Oil Gas Sci Technol Rev IFP 63(5):587–607

George SC, Lisk M, Eadington PJ, Quezada RA, Krieger FW, Greenwood PF, Wilson MA (1996) Comparison of palaeo oil charges with currently reservoired hydrocarbons using the geochemistry of oil-bearing fluid inclusions. Society of Petroleum Engineers, Asia Pacific oil and gas conference, 28–31 October 1996 Adelaide, Australia, pp 159–171

George SC, Ruble TE, Dutkiewicz A, Eadington PJ (2001) Assessing the maturity of oil trapped in fluid inclusions using molecular geochemistry data and visually-determined fluorescence colors. Appl Geochem 16:451–473

George SC, Volk H, Ahmed M (2007) Geochemical analysis techniques and geological applications of oil-bearing fluid inclusions, with some Australian case studies. J Petrol Sci Eng 57:119–138

Gibbs JW (1961) Scientific papers. Dover, New York

Gill WD, Ala MA (1972) Sedimentology of Gachsaran formation (lower Fars series), Southwest Iran. AAPG Bull 56:1965–1974

Glasø O (1980) Generalized pressure–volume–temperature correlations. J Pet Technol 32:785–795

Goldstein RH (1986) Reequilibration of fluid inclusions in low-temperature calcium-carbonate cement. Geology 14:792–795

Goldstein RH, Reynolds TJ (1994) Systematics of fluid inclusions in diagenetic minerals. SEPM short course notes, 31 p

Goldstein RH, Reynolds TJ (1988) Systematics of Fluid Inclusions. In: Diagenetic Minerals: Short course notes. Chevron Oil Field Research, p 40

Hall DL, Sterner SM (1993) Preferential water loss from synthetic fluid inclusions. Contrib Mineral Petrol 114:489–500

Hassanzadeh H, Pooladi-Darvish M, Elsharkawy AM, Keith DW, Leonenko Y (2008) Predicting PVT data for CO_2–brine mixtures for black-oil simulation of CO_2 geological storage. Int J Greenh Gas Control 2:65–77

Head IM, Jones DM, Larter SR (2006) Biological activity in the deep subsurface and the origin of heavy oil. Nature 426:344–352

Hessami K, Koyi HA, Talbot CJ, Tabasi H, Shabanian E (2001) Progressive unconformities within an evolving foreland fold–thrust belt, Zagros Mountains. J Geol Soc Lond 158:969–981

Horsfield B, McLimans RK (1984) Goethermometry and geochemistry of aqueous and oil-bearing fluid inclusions from Fateh Field, Dubai. Org Geochem 6:733–740

Jauber JN, Mutelet F (2004) VLE predictions with the Peng–Robinson equation of state and temperature dependent kij calculated through a group contribution method. Fluid Phase Equilib 224:285–304

Jones DM, Macleod G (2000) Molecular analysis of petroleum in fluid inclusions: a practical methodology. Org Geochem 31(11):1163–1173

Jones DM, Macleod G, Larter SR, Hall DL, Aplin AC, Chen M (1996) Characterization of the molecular composition of included petroleum. In: Brown PE, Hagemann SG (eds) Biennial Pan-American conference on research on fluid inclusions (PACROFI VI), pp 64–65, Wisconsin, USA, Madison

Kamali MR, Rezaee MR (2003) Burial history reconstruction and thermal modeling at Kuh-e-Mond, SW Iran. J Petrol Geol 26:451–464

Karlsen D, Nedkvitne T, Larter SR, Bjorlykke K (1993) Hydrocarbon composition of authigenic inclusions: applications to elucidation of petroleum reservoir filling history. Geochim Cosmochim Acta 57:3641–3659

Katz DL, Firoozabadi A (1978) Prediction phase behavior of condensate /crude oil systems using methane interaction coefficients. J Pet Technol 20:1649–1655

Katz DL, Monroe RR, Trainer RP (1943) Surface tension of crude oils containing dissolved gases. AIME NY, Technical Publication, 1624 p

Larter S, Bowler B, Clarke E, Wilson C, Moffatt B, Bennett B, Yardley G, Carruthers D (2000) An experimental investigation of geochromatography during secondary migration of petroleum performed under subsurface conditions with a real rock. Geochem Trans 9:1–7

Larter S, Huang H, Adams J, Bennett B, Jokanola O, Oldenburg T, Jones M, Head I, Riediger C, Fowler M (2006) The controls on the composition of biodegraded oils in the deep subsurface: part II—geological controls on subsurface biodegradation fluxes and constraints on reservoir-fluid property prediction. AAPG Bull 90(6):921–938

Larter SR, Adams J, Gates I, Bennett B, Huang H (2008) The origin, prediction and impact of oil viscosity heterogeneity on the production characteristics of tar sand and heavy oil reservoir. Petroleum Society's 7th Canadian International Petroleum Conference, p 134

Lin CJ, Kwok YC, Starling KE (1972) Multiproperty analysis of PVT, enthalpy and phase equilibrium data. Can J Chem Eng 50:644

Lisk M, George SC, Summons RE, Quezada RA, O'brien GW (1996) Mapping hydrocarbon charge histories: detailed characterisation of the South Popper Oil Field, Carnarvon Basin. APPEA J 36:445–463

MacGregor AN, Keeney DR (1973) Methane formation by lake sediments during in vitro incubations. JAWRA 9(6):1153–1158

Macleod G, Petch GS, Larter SR, Aplin AC (1993) Investigations of the composition of hydrocarbon fluid inclusions. Abstracts—American Chemical Society 205, p 86

Macleod G, Larter SR, Aplin AC, Petch GS (1994) Improved analysis of petroleum fluid inclusions: application to reservoir studies. Abstract of the ACS 207, p 132

Mango FD (1997) The light hydrocarbons in petroleum: a critical review. Org Geochem 26:417–440

Mauk JL, Burruss RC (2002) Water washing of Proterozoic oil in the midcontinent rift system. AAPG Bull 86:1113–1127

McQuillan H (1985) Fracture controlled production from the Oligo-Miocene Asmari formation in Gachsaran and Bibi Hakimeh fields, southwest Iran. In: Roehl PO, Choquette PW (eds) Carbonate petroleum reservoir. Springer, New York, pp 513–523

Moshtaghian A, Malekzadeh R, Azarpanah (1988) A heavy oil discovery in Islamic Republic of Iran. Paper presented at the fourth UNITAR/UNDP international conference on heavy crude and Tar Sands. Edmonton, AB, Canada, 7–12 August, pp 235–243

Motiei H (1993) Stratigraphy of Zagros. In:Treatise on the geology of Iran. Geological Surveyof Iran Publication.

Motiei H (1994) Geology of Iran: Zagros stratigraphy. Geological Survey of Iran Publications (in Persian), pp 536

Munz IA (2001) Petroleum inclusions in sedimentary basins: systematics, analytical methods and applications. Lithos 55:195–212

Munz IA, Johansen H, Johansen I, Institute for Energy Technology (1999b) Characterisation of composition and PVT properties of petroleum inclusions: implications of reservoir filling and compartmentalisation. SPE 56519, SPE Annual Technical Conference and Exhibition, Houston, Texas, 3–6 October

Munz IA, Johansen H, Holm K, Lacharpagne JC (1999) The petroleum characteristics and filling history of the Frøy field and the Rind discovery. Mar Petrol Geol 16:633–651

Nedkvitne T, Karlsen DA, Bjorlykke K, Larter SR (1993) The relationship between diagenetic evolution and petroleum emplacement in the Ula Field, North Sea. Mar Petroleum Geol 10:255–270

Osjord EH, Rønningsen HP, Tau L (1985) Distribution of weight, density and molecular weight in crude oil derived from computerized capillary GC analysis. High Res Chromatogr Chromatogr Commun 8:683

Pang LSK, George SC, Quezada RA (1998) A study of the gross compositions of oil-bearing fluid inclusions using high performance liquid chromatography. Org Geochem 29:1149–1161

Parnell J (2010) Potential of palaeofluid analysis for understanding oil charge history. Geofluids 10:73–82

Parnell J, Middleton D, Chen H, Hall D (2001) The use of integrated fluid inclusion studies in constraining oil charge history and reservoir compartmentation: examples from the Jeanne d'Arc basin, offshore Newfoundland. Mar Petrol Geol 18:535–549

Pedersen KS, Christensen PL (2006) Phase behavior of petroleum reservoir fluids. CRC Press, Boca Raton

Pedersen KS, Thomassen P, Fredenslund AA (1984) Thermodynamics of petroleum mixtures containing heavy hydrocarbons: 1. Phase envelope calculations by use of the Soave–Redlich–Kwong equation of state. Ind Eng Chem Process Des Dev 23:163–167

Pedersen KS, Thomaasen P, Fredenslund AA (1989) Characterization of Gas Condensate Mixtures. Adv Thermodyn 1:137–152

Pedersen KS, Blilie AL, Meisingset KK (1992) PVT calculations on petroleum reservoir fluids using measured and estimated compositional data for the plus fraction. Ind Eng Chem Res 31(5):1378–1384

Peng DY, Robinson DB (1976) A new two constant equation of state. Ind Eng Chem Fundam 15:59–64

Peneloux A, Rauzy E, Freze R (1982) A consistent correction for Redlich-KwongSoave volumes. Fluid Phase Equilibria 8:7–23

Ping H, Thiéry R (2002) Thermodynamic modeling of petroleum inclusions. Part I: the prediction of the saturation pressure of crude oils. Oil Gas Sci Tech Rev IFP 57(1):1–69

Pironon J, Canals M, Dubessy J, Walgenwitz F, Laplace-Builhe C (1998) Volumetric reconstruction of individual oil inclusions by confocal scanning laser microscopy. Eur J Mineral 10:1143–1150

Roedder E (1984a) Fluid inclusion evidence bearing on the environments of gold deposition. In: Foster RP (ed) Gold 82: the geology, geochemistry and genesis of gold deposits. Balkema, Rotterdam, pp 129–163

Roedder E (1984) Fluid inclusions. Reviews in mineralogy. Mineral Society of America, vol 12

Shafiei A, Dusseault MB, Memarian H, Samimi-Sadeh B (2007) Production technology selection for Iranian naturally fractured heavy oil reserves. In: Proceedings of Canadian International Petroleum Conference (CIPC) 2007 and 58th annual technical meeting held in calgary, Alberta, Canada, 12–14 June 2007

Song YC, Kwon SJ, Woo JH (2004) Mesophilic and thermophilic temperature co-phase anaerobic digestion compared with single-stage mesophilic- and thermophilic digestion of sewage sludge. Water Res 38(7):1653–1662

Standing MB (1952) Volumetric and phase behavior of oilfield hydrocarbon systems. Reinhold, NewYork

Starling KE, Powers JE (1970) Enthalpy of mixtures by modified BWR (Benedict–Webb–Rubin) equation. Ind Eng Chem Fundam 9:531

Stasiuk LD, Snowdon LR (1997) Fluorescence micro-spectrometry of synthetic and natural hydrocarbon fluid inclusions: crude oil chemistry, density and application to petroleum migration. Appl Geochem 12:229–241

Swarbrick RE, Osborne MJ, Grunberger D, Yardley GS, Macleod G, Aplin AC, Larter SR, Knight I, Auld HA (2000) Integrated study of the Judy Field (Block 30/7a)—an overpressured Central North Sea oil/gas field. Mar Petrol Geol 17:993–1010

Taylor P, Larter S, Jones M, Dale J, Horstad I (1997) The effect of oil–water–rock partitioning on the occurrence of alkylphenols in petroleum systems. Geochim Cosmochim Acta 61(9):1899–1910

Thiéry R (2006) Thermodynamic modeling of aqueous CH4-bearing fluid inclusions trapped in hydrocarbon-rich environments. Chem Geol 227:154–164

Thiéry R, Pironon J, Walgenwitz F, Montel F (2000) PIT (petroleum inclusion thermodynamic): a new modeling tool for the characterization of hydrocarbon fluid inclusions from volumetric and microthermometric measurements. J Geochem Explor 69(70):701–704

Thiéry R, Pironon J, Walgenwitz F, Montel F (2002) Individual characterization of petroleum fluid inclusions (composition and P-T trapping conditions) by microthermometry and confocal laser scanning microscopy: inferences from applied thermodynamics of oils. Mar Petrol Geol 19:847–859

Thompson KFM (1979) Light hydrocarbons in subsurface sediments. Geochim Geochim Acta 43:657–672

Thompson KFM (1983) Classification and thermal history of petroleum based on light hydrocarbons. Geochim Geochim Acta 47:303–316

Thompson KFM (1987) Fractionated aromatic petroleums and the generation of gas-condensates. Org Geochem 11:573–590

Thompson KFM (1988) Gas-condensate migration and oil fractionation in deltaic systems. Mar Pet Geol 6:237–246

Tseng HY, Pottorf RJ (2002) Fluid inclusion constraints on petroleum PVT and compositional history of the Greater Alwyn-South Brent petroleum system, North Sea. Mar Pet Geol 19:797–809

Tseng HY, Pottorf RJ, Symington WA (2002) Compositional characterization and PVT properties of individual hydrocarbon fluid inclusions: method and application to hydrocarbon systems analysis. AAPG Annual Convention Official Program, Abstract 11, p A179

Volk H, George SC, Killops SD, Lisk M, Ahmed M, Quezada RA (2002) The use of fluid inclusion oils to reconstruct the charge history of petroleum reservoirs—an example from the Taranaki Basin. In: Proceedings of the New Zealand petroleum conference, Auckland, 24–27 February 2002. Crown Minerals, Auckland, pp 221–233